





Cite this: DOI: 10.1039/c7ta10998a

Reaction mechanisms and sensitivity of silicon nitrocarbamate and related systems from quantum mechanics reaction dynamics†

Tingting Zhou,^{ab} Tao Cheng,^b  Sergey V. Zybin,^b William A. Goddard III *^b and Fenglei Huang^c

Temperature induced instability is an important issue in developing new molecules and materials, but there is no clear understanding about how the molecular structure and crystal packing control sensitivity. This is particularly the case for energetic materials (EMs) important in propulsion and detonation. We propose here the use of quantum mechanics molecular dynamics (QM-MD) based temperature programmed reaction dynamics for predicting the relative sensitivity of various materials while simultaneously obtaining the underlying reaction mechanisms to provide guidance in improving materials. We illustrate this for four closely related molecules, pentaerythritol tetranitrate, pentaerythritol tetranitrocarbamate, and their silicon analogs, that have minor intramolecular differences but exhibit different sensitivities experimentally. Our study finds dramatic differences in reaction mechanisms and energy variation under heating that suggest explanations for the different sensitivities. Important here are both the initial decomposition and the secondary reactions between products. The higher sensitivity of the Si analogs originates from the highly exothermic Si–O bond formation as a paramount initial reaction that promotes other reactions, leading to the generation of various intermediates and final products, thus accelerating the decomposition process and energy release. The nitrocarbamates have low sensitivity because their large complex branching impedes the exothermic Si/C–O bond formation and triggers multiple initial endothermic reaction pathways with higher reaction barriers, delaying secondary exothermic reactions and energy release. We find two computational measures that correlate well with sensitivity: the temperatures at which the energy changes from endothermic to exothermic and the total absorbed energy. This study provides mechanistic insight into the molecular and structural determinants controlling the sensitivity of EMs and provides a practical way to predict the relative sensitivity prior to experimental synthesis and characterization, benefiting the design of novel EMs.

Received 16th December 2017

Accepted 12th February 2018

DOI: 10.1039/c7ta10998a

rsc.li/materials-a

^aInstitute of Applied Physics and Computational Mathematics, Beijing, 100094, P. R. China^bMaterials and Process Simulation Center, California Institute of Technology, 139-74, Pasadena, California, 91125, USA. E-mail: wag@wag.caltech.edu^cState Key Laboratory of Explosion Science and Technology, Beijing Institute of Technology, Beijing, 100081, P. R. China

† Electronic supplementary information (ESI) available: The equilibrium cell parameters for PETN, Si-PETN, PETNC, and Si-PETNC crystals predicted from PBE-D3 calculations at zero temperature are presented in Table S1. Bond order cutoff values for various atom pairs used to identify molecular fragments in PETN, Si-PETN, PETNC, and Si-PETNC are tabulated in Tables S2–S5. Evolution with temperature/time of the reaction products formed during the thermal decomposition of Si-PETN is plotted in Fig. S1. Molecular structures before and after Si–O bond formation during the thermal decomposition of Si-PETN are illustrated in Fig. S2. Evolution with temperature/time of the reaction products formed during the thermal decomposition of PETN is shown in Fig. S3. Evolution with temperature/time of the reaction products formed during the thermal decomposition of Si-PETNC is presented in Fig. S4. Molecular structures before and after Si–O bond formation during the thermal decomposition of Si-PETNC are shown in Fig. S5. Evolution with temperature/time of the reaction products formed during the thermal decomposition of PETNC is plotted in Fig. S6. See DOI: 10.1039/c7ta10998a

1. Introduction

Energetic materials (EMs), including propellants, explosives, and pyrotechnics, are used extensively for a variety of civilian and military applications. Current research on improving EMs focuses on designing and synthesizing novel compounds with high detonation performance (comparable to benchmark EMs such as cyclotetramethylene-tetranitramine (HMX) and cyclotrimethylene-trinitramine (RDX)) while simultaneously reducing sensitivity for safety considerations.^{1–11} However, high energy and low sensitivity requirements are often contradictory, making the development of new EMs difficult and challenging.^{1–11} We aim here to provide synthetic chemists a simple tool for predicting the sensitivity prior to the often complex and time consuming process of synthesizing new generations of EMs.

Sensitivity involves how quickly external stimuli (thermal, impact, friction, electrostatic discharge, or shock) can initiate chemical reactions that lead to decomposition and energy

release. This is a crucial factor that determines the safety and affects the manufacture, transportation, application and storage of these materials.^{1–4,12} A high priority in designing and evaluating proposed new energetic compounds is to minimize sensitivity. Therefore, it is very useful to find a way to predict the factors affecting sensitivity in order to quickly explore new generations of EMs.

It is widely accepted that sensitivity depends upon a complex interplay of various factors such as molecular structure, crystal packing, packing of grains into the test materials, and the nature of the stimulus.^{12–15} Reproducibility of the measured values is notoriously difficult, leading often to contradictory results. At the crystal scale, sensitivity is related to molecular packing mode, anisotropy, and crystal quality parameters such as defects, shape, and size.^{16–22} At the molecular scale, sensitivity is strongly dependent on the molecular composition and geometry configuration.^{1,23–28} For example, sila-pentaerythritol tetranitrate (Si-PETN) shows a dramatically increased sensitivity compared to its carbon analog, pentaerythritol tetranitrate (PETN), although the two molecular structures are nearly identical to each other besides the central atom (silicon *vs.* carbon).^{23–25} δ - and β -HMX have the same molecular composition but different geometry configurations, and the former is more sensitive than the latter.²⁶ Thus even for single crystals the relation between sensitivity and material characteristics is complex and not understood. This becomes even more complex at the mesoscale, where microstructures including grain boundaries, interfaces, surfaces, and voids have an additional influence on the sensitivity of polycrystalline EMs.^{12,29–33}

Recently, the Klapötke group synthesized several nitrocarbamate compounds as potential EMs including the neopentane derivative pentaerythritol tetranitrocarbamate (PETNC) and its silicon analog Si-PETNC.^{27,28} In comparison with the well-known and widely used explosive PETN, PETNC shows an increased thermal stability as well as lower sensitivities against friction and impact.²⁷ Si-PETNC also exhibits higher thermal stability and is much less sensitive to impact as well as friction compared to Si-PETN.²⁸ Si-PETNC is more sensitive than its carbon analog PETNC and matches roughly with the nitrate ester PETN.²⁸

Due to the complexity of factors that might affect sensitivity, previous theoretical studies on predicting sensitivity have generally tried to find correlation with a single molecular or crystal property of EMs, such as oxygen balance, molecular electronegativity, partial atomic charge, electrostatic potentials, weakest bond dissociation energy, band gap, free space per molecule, crystal packing mode, *etc.*^{34–45} Despite significant efforts and many suggested empirical correlations, no clear understanding has been achieved regarding the relationships between the sensitivity of materials, their molecular and crystalline structures, and chemical properties.^{36,46}

We consider that four compounds, Si-PETN, PETN, Si-PETNC, and PETNC, provide a good challenge to develop an understanding of the molecular and structural determinants controlling their sensitivity to external stimuli. This is because PETN, PETNC, and Si-PETNC have exactly the same space group, $P\bar{4}21c$, with minor differences in their molecular

structure.^{27,28,47} Although the experimental crystal structure of Si-PETN is unavailable, we assume that it is also similar since the molecular structures of Si-PETN and PETN are nearly the same besides the central atom.²³ The molecular and crystal structures of the four EMs are shown in Fig. 1. Our previous theoretical studies^{24,25} on the decomposition mechanisms of PETN and Si-PETN elucidated how the replacement of the central C by Si dramatically increases the sensitivity of Si-PETN. In the current work, we use quantum mechanics molecular dynamics (QM-MD) to predict the thermal decomposition mechanisms and sensitivity of condensed phase Si-PETN, PETN, Si-PETNC, and PETNC.

We aim here to uncover the complex chemical processes underlying thermal initiation and the reasons for the lower sensitivity of nitrocarbamate compounds and for the higher sensitivity of their silicon analogs. Then we want to find a simple method to predict the relative sensitivity of EMs. The problems associated with characterizing and measuring sensitivity suggest that seeking precise structure/activity correlations is unrealistic except on a very limited scale.³⁷ Accordingly, our goal is to try to understand the molecular determinants that influence sensitivity, and then to make meaningful predictions of relative sensitivities. This should help provide clues useful for understanding sensitivity of other systems to aid molecular design of novel EMs with tailored properties. Moreover, the chemical reaction mechanism and kinetics including the energy release are essential to developing thermochemical models useful in hydrodynamic simulations of these materials.

This is the first report of QM-MD studies of the reaction mechanisms and thermal sensitivity of solid Si-PETN, PETN, Si-PETNC, and PETNC. We used the PBE-D3 flavor of the generalized gradient approximation to density functional theory (DFT) with periodic boundary conditions. The details of computational methods are given in Section 2. The simulated results are presented and discussed in Section 3. Conclusions are drawn in Section 4.

2. Methodology

The QM calculations use the interatomic forces calculated in the framework of density functional theory (DFT),⁴⁸ where exchange and correlation are treated with the generalized gradient approximation (GGA) using the Perdew–Burke–Ernzerhof (PBE) functional form.⁴⁹ The London dispersion was corrected using the D3 method with Becke–Jonson damping.⁵⁰ The Vienna *Ab initio* Simulation Package (VASP)⁵¹ ported to a GPU was employed to perform these periodic QM simulations.

Since there is no experimental crystal structure for Si-PETN and the difference between Si-PETN and PETN molecules is the central atom type, we first replaced the central C in PETN with Si and optimized the molecular and crystal structures using the conjugate gradient methodology to obtain the Si-PETN crystal. The energy cutoff for the plane wave expansion was set to 600 eV. Convergence is reached if the energy and force differences are within 1×10^{-6} eV for electronic iterations and 1×10^{-4} eV \AA^{-1} for ionic relaxations, respectively. The reciprocal space was sampled with the Γ -centered Monkhorst–Pack

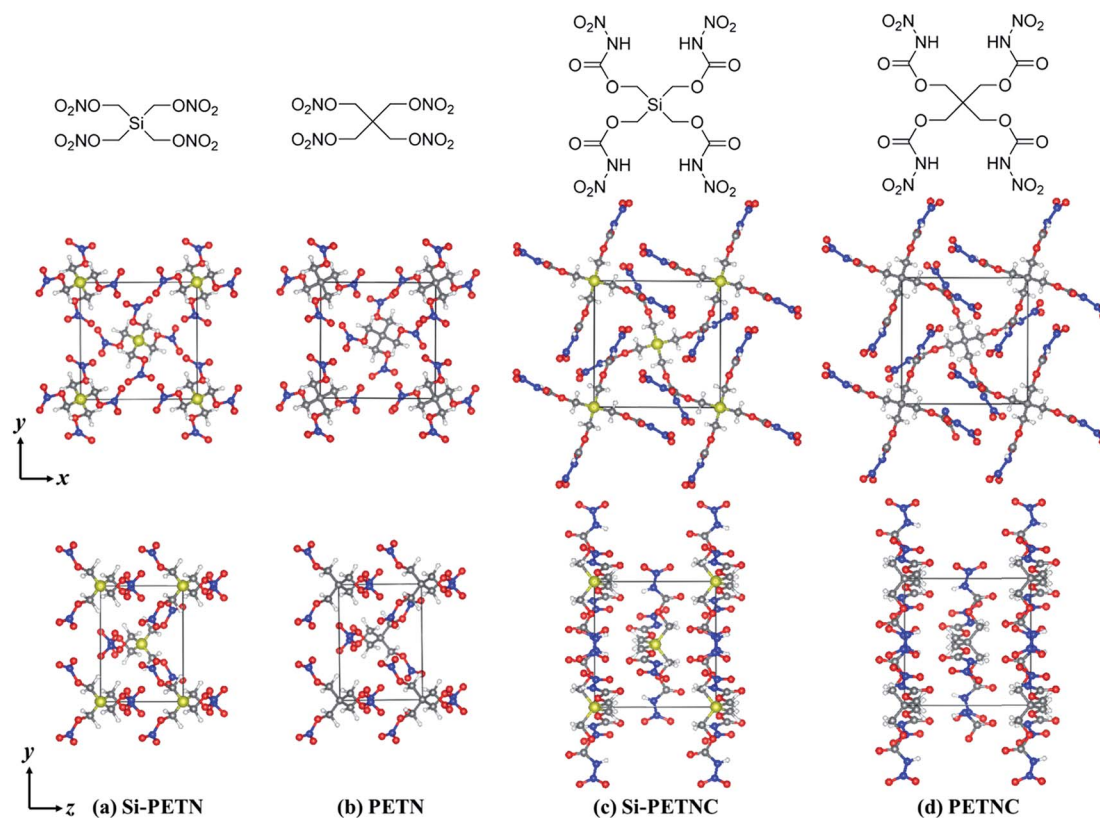


Fig. 1 The molecular and crystal structures of PETN, Si-PETN, PETNC, and Si-PETNC. The crystal structures shown on the top are viewed along the *c* axis, and the ones at the bottom are along the *a* axis. The C, H, N, O, and Si atoms are represented by gray, white, blue, red, and yellow balls, respectively.

scheme using $3 \times 3 \times 5$ gamma points. For consistency, the other three experimental crystal structures were also relaxed at the same computational level. The cell parameters of the optimized crystal structures are summarized in Table S1 of the ESI,[†] showing excellent agreement with the available experimental and theoretical results.^{33,34,47,53} These optimized unit cells were then replicated twice so that each has four molecules per periodic cell for the MD simulations.

DFT-MD simulations were then performed to investigate the reaction mechanisms of thermal decomposition under heating. The systems were first heated from 20 K to 300 K within 2 ps, followed by equilibration at 300 K for 2 ps. They were finally heated continuously from 300 K to 3000 K over 20 ps (at a heating rate of 135 K ps^{-1}). The NVT ensemble (constant temperature, constant volume, and constant number of atoms) was used, and the temperature was controlled using the Nose–Hoover thermostat with a time constant of 50 fs. A time step of 1 fs for integrating the equations of motion was applied. The MD trajectories were saved every 10 fs and used to analyze reaction mechanisms. The high temperatures used in these MD simulations allow many reactions to be observed within the practical time scale of DFT-MD of 20 ps. For these supercell DFT-MD simulations, the energy cutoff for the plane wave expansion was reduced to 500 eV. The convergence criteria were 1×10^{-5} eV for the energy difference and $1 \times 10^{-3} \text{ eV \AA}^{-1}$ for the force difference. Only the gamma point of the reciprocal space was sampled.

To identify the reaction products formed during thermal decomposition, we determined the atom connectivity using bond order cutoffs. The algorithm is the same as that used in previous studies of reactive molecular dynamics simulations.⁵² Any two fragments are considered as separate molecules if all bonds between them have bond orders smaller than the cutoff values. After determining the molecular fragments, the molecular recognition algorithm assigns a unique identification number to each fragment to trace the reaction pathways. The cutoffs for various atom pairs (tabulated in Tables S2–S5 of the ESI[†]) are confirmed by comparing the analyzed products with the molecular structures in the decomposed crystals from the MD trajectories. We used a time window of 0.2 ps to avoid confusion due to short-term fluctuations in the bonds above and below the cutoff, that is, the bond must be maintained for at least 0.2 ps to be considered as a bond.

3. Results and discussion

3.1 Reaction mechanisms for the nitro esters Si-PETN and PETN

3.1a. Si-PETN. The initiation of thermal decomposition of Si-PETN occurs through O–NO₂ bond cleavage when the temperature increases to 1543 K ($t = 9.21 \text{ ps}$), leading to the formation of NO₂. Then the Si–CH₂O bond breaks immediately after NO₂ dissociation, generating CH₂O at 1549 K ($t = 9.25 \text{ ps}$).

Next we find the formation of the Si–O bond as the temperature reaches 1562 K ($t = 9.35$ ps). The mechanisms of these first three initial reactions are illustrated in Fig. 2, showing that for all four intact Si-PETN molecules, the first reaction step is always O–NO₂ bond rupture followed by Si–CH₂O bond breakage in the same branch. Previous static QM calculations on a single Si-PETN molecule²⁴ suggested that the barrier for CH₂O dissociation is 48.2 kcal mol^{−1}, which is 12.6 kcal mol^{−1} higher than that for NO₂ release, explaining why CH₂O always forms after NO₂.

The Si–O bond formation is of paramount importance in the initial reactions since it leads to massive energy release (−44.5 kcal mol^{−1}),²⁴ which can promote other reactions to accelerate the decomposition process. The first two Si–O bonds ($t = 9.35$ and 10.28 ps) are formed due to the attraction between the central Si and the O in the dissociated CH₂O. We observe the bending of Si–CH₂–O after NO₂ dissociation and before CH₂O elimination, resulting in the extension of the Si–C bond while decreasing the distance of the O from the central Si. The subsequent CH₂O dissociation is similar to the transition state of the rearrangement of Si–CH₂–O predicted from QM calculations.²⁴ The Si–O bond formed at 11.08 ps involves the rearrangement of Si–CH₂–O in the branch after losing NO₂. The

attraction between the central Si and one O in the dissociated NO₂ leads to the formation of Si–O bonds at 11.26 and 11.41 ps.

The number of Si–O bonds increases continuously as the temperature increases and a rapid increment begins after the temperature approaches 1796 K ($t = 11.08$ ps), as shown in Fig. S1(a).† The reaction pathways leading to the formation of Si–O bonds are presented in Table 1 and the molecular structures before and after Si–O bond formation are illustrated in Fig. S2 of the ESI,† from which detailed information about the reaction mechanisms can be derived. Mechanism one is the attraction between the central Si and the O in dissociation fragments such as CH₂O, NO₂, NO₃, CNO₃, and CHO₂. The Si–O bonds formed at 9.35, 10.28, and 12.59 ps arise from the attraction between Si and O in the dissociated CH₂O. The attraction between Si and one O in the split NO₂ leads to the formation of Si–O bonds at 11.26, 11.41, 12.07, 12.29, and 13.22 ps. The Si–O bonds formed at 13, 13.49, and 14.27 ps arise from the attraction between Si and O in the dissociated NO₃, CNO₃, and CHO₂, respectively. Mechanism two involves the rearrangement of Si–CH₂–O in the branches after losing NO₂, forming the Si–O bonds at 11.08 and 11.76 ps. Mechanism three is the attraction between Si and one O in –NO₂. The Si–O bond formed at 11.39 ps is due to intermolecular attraction and the

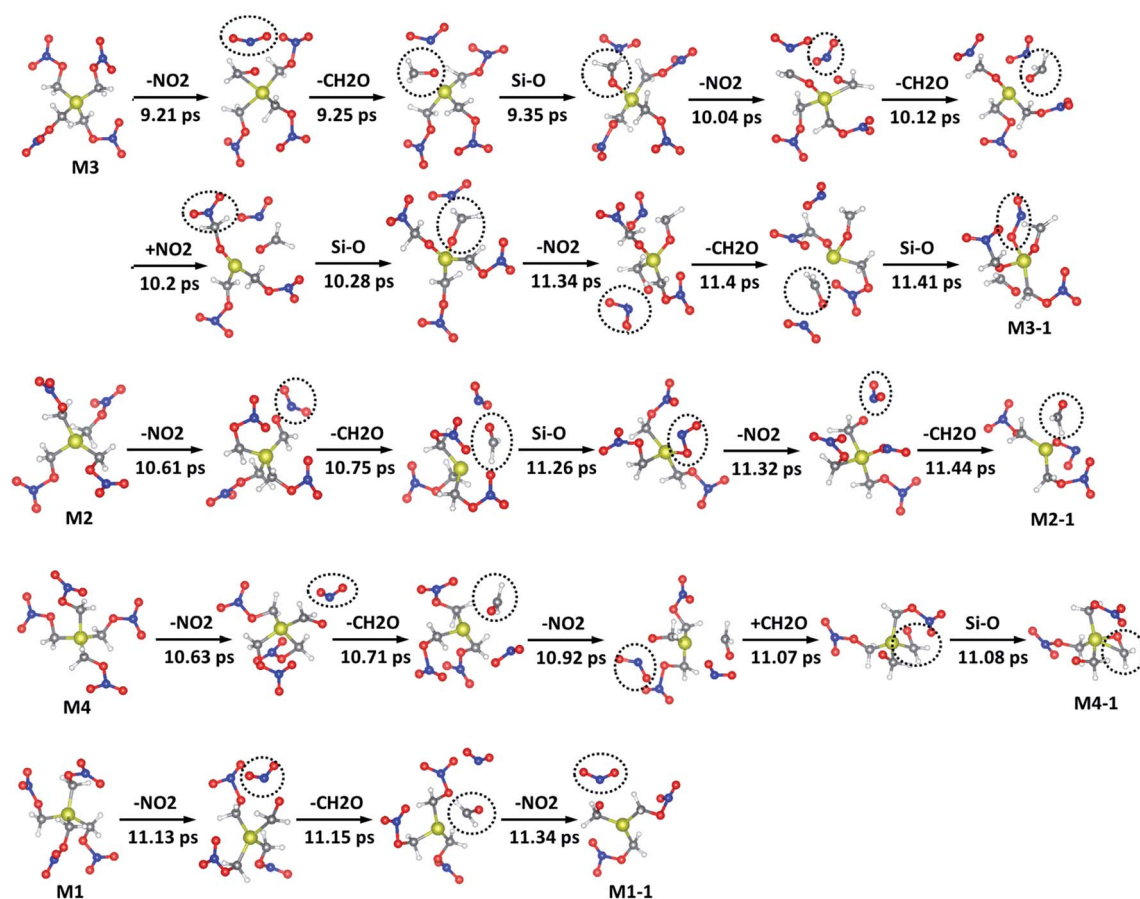


Fig. 2 Reaction process of initial reactions during the thermal decomposition of Si-PETN. The C, H, N, O, and Si atoms are represented by gray, white, blue, red, and yellow balls, respectively. The four intact Si-PETN molecules are represented by M1, M2, M3, and M4. The partially decomposed Si-PETN molecules after these reactions are represented by M1-1, M2-1, M3-1, and M4-1.

Table 1 Reaction pathways and the corresponding time and temperature leading to Si–O bond formation in the Si-PETN crystal during the heating process^a

Products	Reaction pathways	<i>t</i> (ps)	<i>T</i> (K)
Si–O bond	CH ₂ O (7) + C ₃ H ₆ N ₃ O ₉ Si (8) → C ₄ H ₈ N ₃ O ₁₀ Si (9)	9.35	1562
	C ₃ H ₆ N ₃ O ₈ Si (13) + CH ₂ O (12) → C ₄ H ₈ N ₃ O ₁₀ Si (15)	10.28	1688
	C ₄ H ₈ N ₂ O ₈ Si (26) → C ₄ H ₈ N ₂ O ₈ Si (27)	11.08	1796
	C ₃ H ₆ N ₃ O ₉ Si (23) + NO ₂ (16) → C ₃ H ₆ N ₄ O ₁₁ Si (34)	11.26	1820
	C ₃ H ₆ N ₂ O ₇ Si (39) + C ₃ H ₆ N ₂ O ₇ Si (29) → C ₆ H ₁₂ N ₄ O ₁₄ Si ₂ (41)	11.39	1838
	C ₃ H ₆ N ₂ O ₇ Si (43) + NO ₂ (10) → C ₃ H ₆ N ₃ O ₉ Si (44)	11.41	1840
	C ₆ H ₁₂ N ₂ O ₁₁ Si ₂ (72) → C ₆ H ₁₂ N ₂ O ₁₁ Si ₂ (77)	11.76	1888
	C ₆ H ₁₁ N ₂ O ₁₁ Si ₂ (83) + NO ₂ (35) → C ₆ H ₁₁ N ₃ O ₁₃ Si ₂ (90)	12.07	1929
	C ₂ H ₄ NO ₅ Si (95) → C ₂ H ₄ NO ₅ Si (97)	12.13	1938
	C ₅ H ₉ NO ₁₀ Si ₂ (105) + NO ₂ (18) → C ₅ H ₉ N ₂ O ₁₂ Si ₂ (111)	12.29	1959
	C ₅ H ₉ N ₂ O ₁₂ Si ₂ (111) → C ₅ H ₉ NO ₉ Si ₂ (112) + NO ₃ (113)	12.30	1961
	C ₄ H ₁₀ NO ₈ Si ₂ (120) → C ₃ H ₈ NO ₇ Si ₂ (122) + CH ₂ O (121)	12.48	1985
	CH ₂ O (32) + C ₂ H ₂ O ₃ Si (79) → C ₃ H ₄ O ₄ Si (123)	12.59	2000
	C ₃ H ₈ NO ₇ Si ₂ (122) + NO ₃ (113) → C ₃ H ₈ N ₂ O ₁₀ Si ₂ (131)	13.00	2055
	CH ₂ O ₃ Si (142) + NO ₂ (38) → CH ₂ NO ₅ Si (149)	13.22	2085
	CH ₂ NO ₅ Si (149) + CNO ₃ (158) → C ₂ H ₂ N ₂ O ₈ Si (160)	13.49	2121
	C ₂ H ₆ NO ₅ Si (210) + CHO ₂ (172) → C ₃ H ₇ NO ₇ Si (211)	14.27	2226

^a The numbers in parentheses are the identifications (ID) of fragments.

ones at 12.13 and 12.3 ps are due to intramolecular attraction. In the fragment with two Si, the O in the Si–O bond formed at 12.3 ps also bonds to the other Si at *t* = 12.48 ps. The attraction between the central Si and the O in dissociation fragments plays a dominant role in the formation of the Si–O bond. After losing one branch (NO₂ and CH₂O) in the Si-PETN molecule, the central Si atom connected with three atoms becomes more active than the original state with four atoms. And the cleavage of the branch leaves more free space and exposes the central Si to other fragments, making it easier to attract the O in dissociated products and form the Si–O bond.

Static QM calculations²⁴ suggested that the Si–O bond formation *via* a carbon-silyl nitro-ester rearrangement (R3Si–CH₂–O–R2 → R3Si–O–CH₂–R2) should be the first reaction step due to its lower barrier than O–NO₂ bond cleavage (reaction enthalpy: 32.0 vs. 35.6 kcal mol^{−1}). However, our QM dynamical simulation under a constant heating rate shows that the Si–CH₂–O rearrangement occurs after O–NO₂ bond breaking. This is because the rearrangement has a very tight transition state (very low entropy) which is disfavored at higher temperatures. Experiments exposing the crystal to a high-energy laser, high-energy fracture, or high pressure found that Si–C/C–C and C–O bonds were the first to break, which was interpreted to suggest that the O–NO₂ bond is relatively stronger than these other bonds.^{54–56} In contrast, we find that slower thermal decomposition leads to O–NO₂ bond rupture as the initial step, which was also observed for low-energy fracture or low-energy laser exposure at ambient pressures.^{55,57}

As the temperature increases above 1850 K, we observe the formation of NO, H, and HONO. The NO₂ attracted by the central Si atom breaks one O–N bond, leading to the elimination of NO at an early stage. The NO formed at a later time is due to the further decomposition of other products (*e.g.*, HONO, N₂O₃, and the fragment with two Si formed by the combination of two partially decomposed Si-PETN molecules). H atoms are

mainly dissociated from the partially decomposed Si-PETN and from the decomposition of other products (*e.g.*, HONO and HNO). The secondary reaction between dissociated NO₂ and H contributes greatly to the formation of HONO, which is also split from the fragment with two Si and from the partially decomposed Si-PETN. Although QM calculations of the adiabatic energy surfaces suggested that HONO might be an initial reaction product, because the reaction barrier is only 3.8 kcal mol^{−1} higher than that for NO₂ dissociation,²⁴ our MD simulations indicate that HONO is not eliminated directly from the original Si-PETN molecule, and it forms much later and at a higher temperature than NO₂, CH₂O, and the Si–O bond.

The onset of various secondary exothermic reactions between decomposition products leads later to the formation of many intermediate products (such as HO, CH₂O₂, HNO, CHO₂, CNO, and CHNO) and final products (such as CO, H₂O, N₂O, and CO₂). These exothermic reactions are critical since they contribute to the energy release that accelerates the decomposition process. The observed rate increase as the decomposition continues shows that reactions between decomposition products accelerate decomposition with possible autocatalytic effects.^{58–60} The time evolution of the major reaction products formed during the thermal decomposition of Si-PETN is presented in Fig. S1 of the ESI.†

3.1b. PETN. In the heating induced decomposition of PETN, the first reaction step is also O–NO₂ bond fission when the temperature approaches 2078 K (*t* = 13.17 ps), which is ~540 K higher (~4 ps later) than that for Si-PETN, indicating that PETN is much more stable. The next reactions are the elimination of HONO and H at the same time (*T* = 2087 K, *t* = 13.24 ps), immediately after the dissociation of NO₂. Very quickly, in another 0.14 ps (*T* = 2097 K, *t* = 13.31 ps), we find that the C–CH₂O bond breaks leading to the formation of CH₂O. The reaction processes with regard to the four initial reaction products are illustrated in Fig. 3, showing that the initiation of

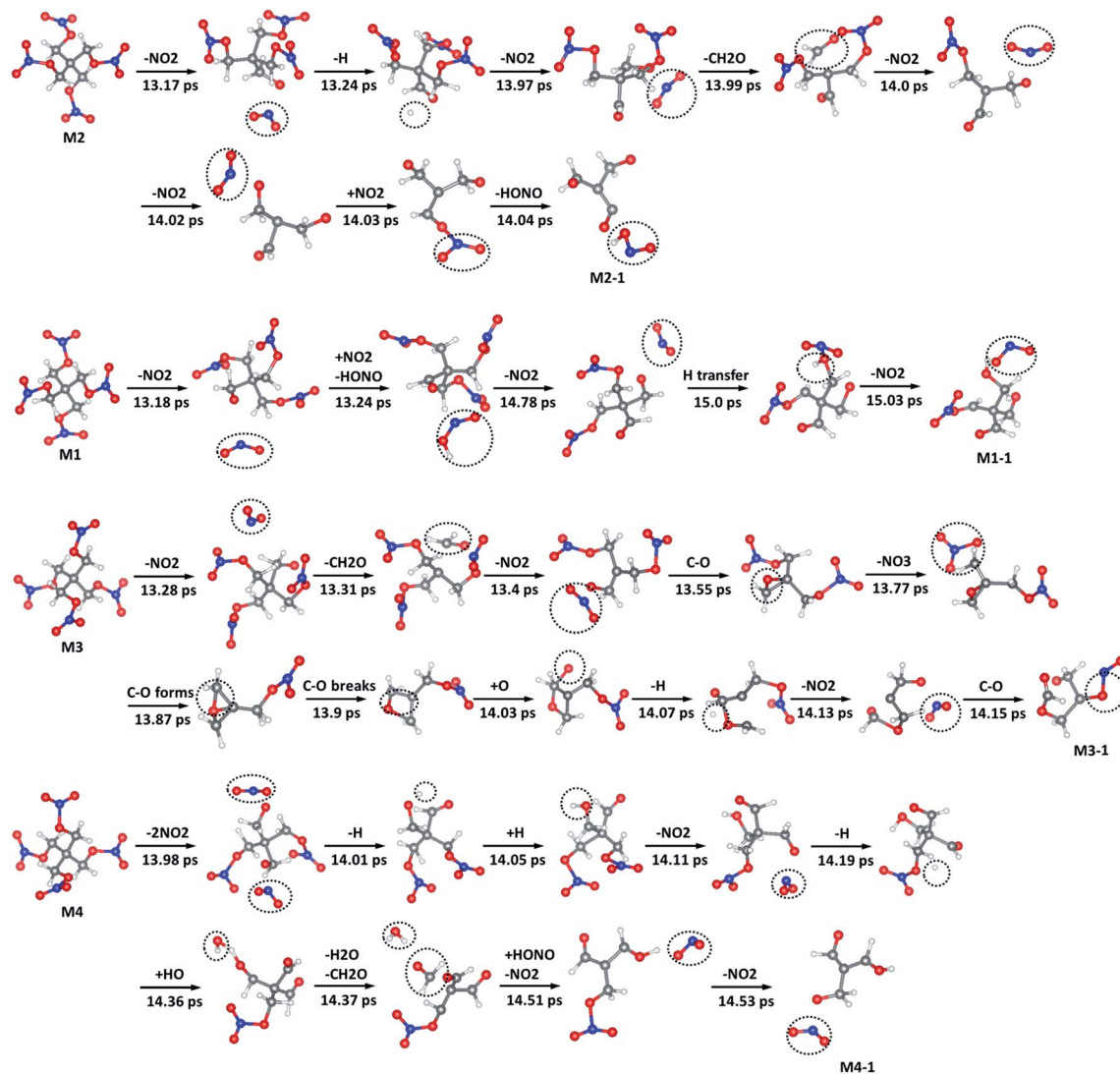


Fig. 3 Reaction process of initial reactions during the thermal decomposition of PETN. The C, H, N, and O atoms are represented by gray, white, blue, and red balls, respectively. The four intact PETN molecules are represented by M1, M2, M3, and M4. The partially decomposed PETN after these reactions are represented by M1-1, M2-1, M3-1, and M4-1.

thermal decomposition is always through O–NO₂ bond cleavage for all four intact PETN molecules. The subsequent reaction between dissociated NO₂ and the H in partially decomposed PETN or dissociated H leads to the formation of HONO. Both H and CH₂O are eliminated from the branch after losing NO₂. Static QM calculations on a single PETN molecule²⁴ found that the barrier for HONO elimination is essentially the same as that for O–NO₂ bond cleavage (39.2 vs. 39.0 kcal mol^{−1}). However, our dynamical simulation under heating shows that HONO is always formed after NO₂ and is not dissociated directly from the intact PETN molecule. The barrier for CH₂O dissociation is about 10 kcal mol^{−1} higher (49.1 kcal mol^{−1}),²⁴ which is consistent with the delayed occurrence compared to the formation of NO₂ and HONO.

The rearrangement of C–CH₂–O (R3C–CH₂–O–R2 → R3C–O–CH₂–R2) leading to the formation of a C–O bond was suggested to be impossible due to the extremely high barrier

(80.1 kcal mol^{−1}).²⁴ Indeed, we only observe one similar rearrangement at 2129 K ($t = 13.55$ ps) in the branch after losing NO₂ in the partially decomposed PETN (molecular ID: M3), as illustrated in Fig. 3. The central C atom simultaneously bonds to the C and O in –CH₂O, forming four bonds. After 0.32 ps, the C atom belonging to –CH₂ in another branch also bonds to the O in –CH₂O, leading to the immediate rupture of the C–O bond formed *via* the C–CH₂–O rearrangement. The second C–O bond is formed at 2210 K ($t = 14.15$ ps) through the attraction between the central C and one O in the dissociated NO₂ in M3. These are the only two C–O bonds formed during the whole decomposition process of PETN. Therefore, C–O bond formation does not play an important role in the decomposition of PETN, although this reaction is exothermic (−13.5 kcal mol^{−1} (ref. 24)). This is the significant difference between the initial reactions of Si-PETN and PETN. For Si-PETN, the formation of many Si–O bonds releases a great deal of energy, dramatically

accelerating the decomposition process and dramatically enhancing the sensitivity of Si-PETN.

When the temperature increases to higher values than 2200 K, the formation of NO, HNO, and HO is observed. The further decomposition of PETN moieties and initial products such as HONO and NO₂ generates NO. The secondary reaction between NO and the released H or the H in other products leads to the formation of HNO. HO is mainly generated from the decomposition of HONO. Other intermediate products, including CHO₂, CH₂O₂, and N₂O₂, are formed later due to secondary reactions between products and the further decomposition of other fragments. The thermal decomposition of PETN generates final products such as H₂O, CO₂, CO, N₂O, and N₂. The time evolution of the major reaction products formed during the thermal decomposition of PETN is plotted in Fig. S3 of the ESI.†

3.2 Reaction mechanisms for the nitrocarbamates Si-PETNC and PETNC

3.2a. Si-PETNC. The first reaction step for Si-PETNC is intermolecular hydrogen transfer between two Si-PETNC molecules (M2 and M3), as shown in Fig. 4. The intermolecular H transfer starts as the temperature reaches 1676 K ($t = 10.19$ ps). The O belonging to -CO in one Si-PETNC attracts the H belonging to -NH in an adjacent Si-PETNC, forming Si-PETNC - H and Si-PETNC + H simultaneously. Then, one O belonging to -NO₂ in Si-PETNC - H attracts the H belonging to -NH in Si-PETNC + H at 1685 K ($t = 10.26$ ps), leading to the formation of two new Si-PETNC molecules with a modified molecular structure compared to the intact Si-PETNC molecule. After 0.4 ps ($t = 10.66$ ps, $T = 1739$ K), the H attracted by -NO₂

returns to its donor and the H captured by -CO also bonds to its donor, resulting in the formation of a homo-dimer. This dimer disappears immediately due to the bond breaking of N-H ($t = 10.67$ ps, $T = 1740$ K), forming again Si-PETNC - H and Si-PETNC + H. After 0.14 ps ($t = 10.81$ ps, $T = 1759$ K), the H belonging to -NH in another branch of Si-PETNC - H transfers to the O belonging to -CO in another branch of Si-PETNC + H, leading to the generation of Si-PETNC - 2H and Si-PETNC + 2H. This H immediately returns to its donor and connects with one O in -NO₂, forming Si-PETNC - H and Si-PETNC + H for the third time ($t = 10.82$ ps, $T = 1761$ K). At $t = 11.27$ ps ($T = 1821$ K), the H connected with -CO in Si-PETNC + H also bonds to its donor, forming a hetero-dimer. The O-H bond breaks immediately, resulting in two Si-PETNC molecules ($t = 11.28$, $T = 1823$ K). At this point, the intermolecular hydrogen transfer process is completed. In summary, the H transfer is mainly between -NH and -CO or between -NH and -NO₂. The final configurations of the two Si-PETNC molecules after intermolecular H transfer are as follows: one Si-PETNC (M3) returns to its original configuration and in another Si-PETNC (M2) the H initially connected with -N bonds to one O in -NO₂. We did not observe such H transfer for the other two Si-PETNC molecules (M1 and M4).

As the temperature increases above 1966 K ($t = 12.34$ ps), intramolecular hydrogen transfer between -OH and -CO occurs in the Si-PETNC molecule with the new configuration (M2-1). As shown in Fig. 5, the H bonding to one O in -NO₂ also connects with the adjacent O belonging to -CO in the same branch. Then, the original H-O bond breaks and the H transfers entirely to the O in -CO at 1994 K ($t = 12.55$ ps). After 2.55 ps ($t = 15.1$ ps, $T =$

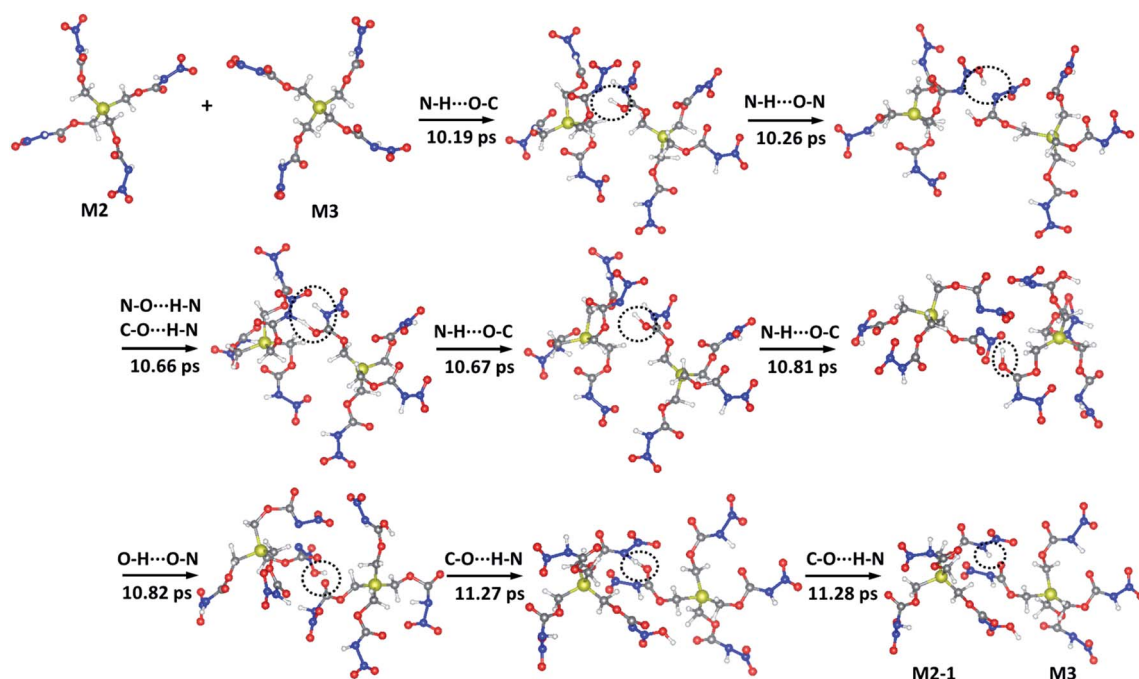


Fig. 4 Reaction process of intermolecular H transfer during the thermal decomposition of Si-PETNC. The C, H, N, O, and Si atoms are represented by gray, white, blue, red, and yellow balls, respectively. The intermolecular hydrogen transfer occurs between two Si-PETNC molecules, M2 and M3. After H transfer, M3 returns to its original configuration and M2 is converted to M2-1.

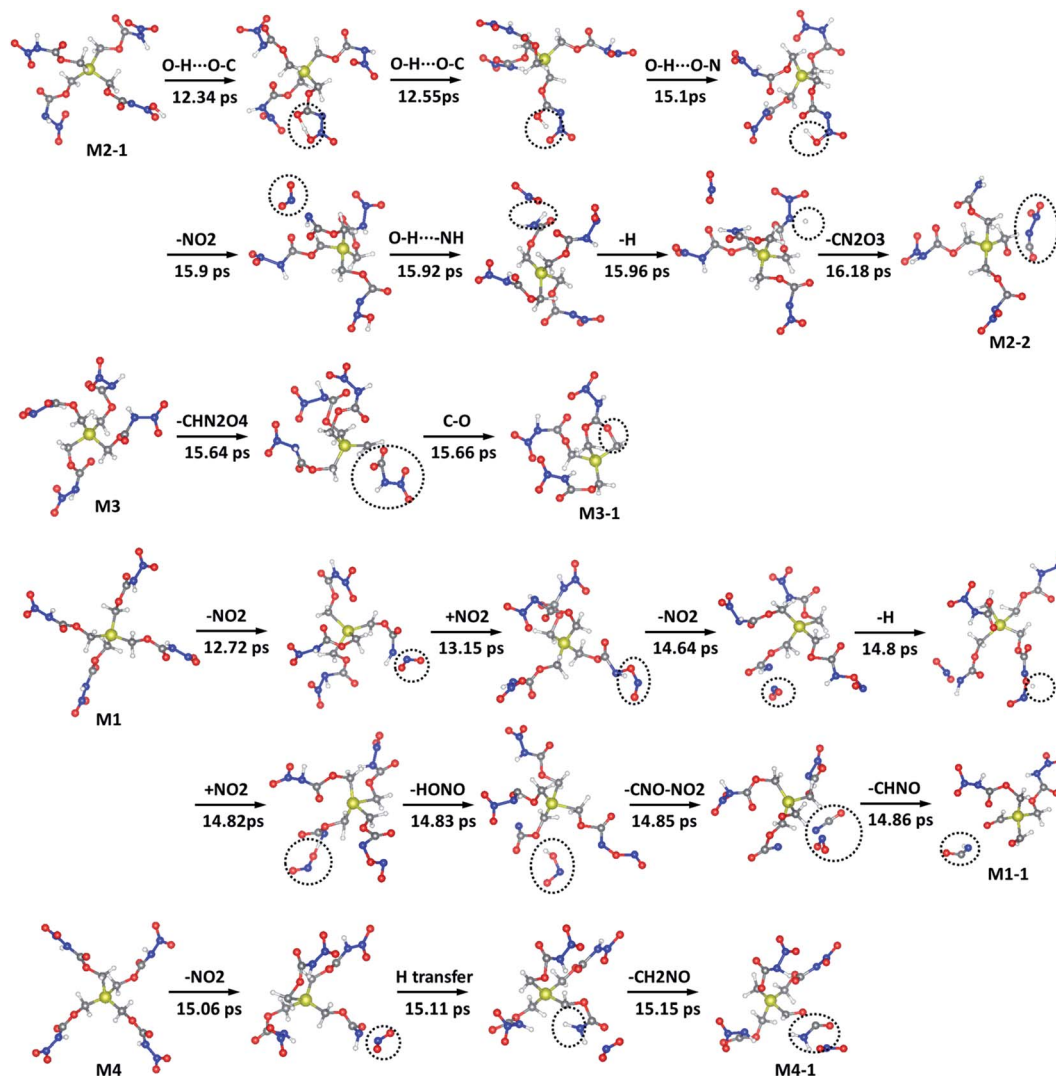


Fig. 5 Reaction process of initial reactions during the thermal decomposition of Si-PETNC. The C, H, N, O, and Si atoms are represented by gray, white, blue, red, and yellow balls, respectively.

2339 K), the H returns to its donor and this molecular configuration remains until the onset of N-NO₂ bond breaking in another branch when the temperature reaches 2447 K ($t = 15.9$ ps). The intramolecular H transfer promotes neither HONO elimination nor HO dissociation.

Although H transfer occurs very early in the decomposition process of Si-PETNC, it does not catalyze other reactions. We did not observe any other reactions during the procedure of intermolecular or intramolecular H transfer and the following decomposition reactions for both of the two Si-PETNC molecules occur later than those for the other two Si-PETNC molecules (M1 and M4) without H transfer. As shown in Fig. 5, the decomposition of M1 begins at 12.72 ps, which is ~ 3 ps earlier, and the corresponding temperature is 2017 K, which is ~ 400 K lower than those for M2 and M3. The decomposition of M4 starts ~ 0.7 ps earlier and the temperature is ~ 100 K lower than those for M2 and M3. Therefore, we consider that the back and forth H transfer as an initial reaction does not accelerate the decomposition of Si-PETNC.

The initiation of M3 decomposition occurs *via* CH₂-O bond rupture dissociating CHN₂O₄, while the decomposition of the other three Si-PETNC molecules begins through N-NO₂ bond cleavage forming NO₂. The first dissociated NO₂ at 12.72 ps is consumed after 0.43 ps due to the bonding between the O and the N in -NH. This branch further eliminates H, NO₂, and CNO during the next 1.7 ps. The second NO₂ is eliminated from another branch in the same Si-PETNC molecule at 14.64 ps ($T = 2276$ K), which is quickly consumed due to the bonding between the O and the H in -NH, favoring the immediate dissociation of HONO and CHNO from this branch. Therefore, the reactions following N-NO₂ bond cleavage include the dissociation of H, HONO, CNO, and CHNO. These reactions occur sequentially and with very short time intervals, indicating that they are closely correlated with each other. For some reactions, the product of the previous step is the reactant of the next step. The reaction details of these initial products and their evolution with temperature/time are described in Fig. S4 of the ESI.†

As the temperature increases above 2353 K ($t = 15.21$ ps), we see Si–O bond formation. The exothermicity of this reaction makes it critical to the initial decomposition process. The number of Si–O bonds increases continuously with the increase of temperature, with a more rapid increment after 2596 K ($t = 17.01$ ps) as shown in Fig. S4(a) of the ESI.† It reaches a maximum of 13 at 2811 K ($t = 18.6$ ps) and then decreases to 11 over the next 1.4 ps. The reaction pathways with regard to Si–O bond formation are tabulated in Table 2 and the molecular structures before and after Si–O bond formation are shown in Fig. S5 of the ESI.† The mechanisms for Si–O bond formation in Si-PETNC are similar to those in Si-PETN: the rearrangement of Si–CH₂–O in the branch after losing –CONHNO₂, the attraction between the central Si and the O in dissociated fragments, and the intermolecular attraction between the Si and the O in –CH₂O. Mechanism one leads to the formation of a Si–O bond at 15.21 ps. The Si–O bonds formed at 15.49 and 17.75 ps are due to the Si attracting the O in the dissociated HO. The attractions between Si and the O in the dissociated CH₂O lead to the formation of Si–O bonds at 16.33 and 17.87 ps. The Si–O bonds formed at 16.48, 16.8, 17.54, 17.61, 17.68, 18.19, and 18.60 ps arise from attractions between Si and one O in CHN₂O₄, C₃H₄NO₄, HONO, NO₂, C₂H₂NO₂, CH₂O₂, and C₂H₃O, respectively. The Si in the thoroughly decomposed Si-PETNC (M2) attracts the O belonging to –CH₂O in the adjacent Si-PETNC residue (M3), forming a Si–O bond at 17.21 ps. The attraction between the central Si and the O in the dissociated products plays a dominant role in the formation of the Si–O bond in Si-PETNC, the same as that for Si-PETN.

For Si-PETNC, the formation of the Si–O bond begins later and at a higher temperature than the dissociation of NO₂, H, HONO, CNO, and CHNO. Moreover, all Si–O bonds are formed in the partially decomposed Si-PETNC, most of which are highly decomposed. In comparison with Si-PETN, the Si–O bond formation in Si-PETNC begins at a temperature ~800 K higher (~5.9 ps later) and the number is smaller. As shown in Fig. 1, the branch in the original Si-PETNC molecule is much longer than that for Si-PETN, making it more difficult to bend and

form a five-coordinate Si as a transition state of Si–CH₂–O rearrangement. This large branch also impedes contact between the central Si and the dissociated fragments; therefore, most of the attractions between the Si and the O in dissociated fragments occur in the highly decomposed Si-PETNC at a later time. Consequently, the roles of Si–O bond formation in the initial reactions and in enhancing the sensitivity of Si-PETNC are much less significant than for Si-PETN.

With the continuous increase in temperature, we observe HO, NO, CHN₂O₄, CH₂O, and CH₂O₂. The decomposition of initial product HONO contributes significantly to the formation of HO and NO. HO is also generated from the further decomposition of Si-PETNC moieties and the secondary reactions between other products. NO is also formed due to the decomposition of NO₂, Si-PETNC moieties, and the fragment with two Si. CHN₂O₄ is first dissociated from Si-PETNC (M3) and then from further decomposition of Si-PETNC after losing H, NO₂, and CHNO. We do not consider CHN₂O₄ as a crucial initial product since it forms later than other initial products and the amount is small. CH₂O and CH₂O₂ are formed mainly due to the decomposition of and the secondary reactions between other products. Compared to Si-PETN, CH₂O forms at a much higher temperature and the reaction mechanisms are significantly different for Si-PETNC. The final products formed during the thermal decomposition process of Si-PETNC include H₂O, CO, N₂O, CO₂, and N₂. The time evolution of the major reaction products formed during the thermal decomposition of Si-PETNC is shown in Fig. S4 of the ESI.†

3.2b. PETNC. The initial reactions during the thermal decomposition of PETNC include the dissociation of C₂H₃N₂O₄ and CHN₂O₄, hydrogen transfer, and the formation of H, NO₂, C₂H₃NO₂, and CHNO, as shown in Fig. 6. For M1, the first reaction step is the dissociation of C₂H₃N₂O₄ due to C–CH₂ bond fission when the temperature increases to 2120 K ($t = 13.48$ ps). C₂H₃N₂O₄ is unstable, and quickly decomposes into C₂H₃NO₂ and NO₂, and the former immediately decomposes into CH₂O and CHNO. This CH₂O soon decomposes to H and CHO. Although C₂H₃N₂O₄ forms earlier than the other products, this is

Table 2 Reaction pathways and the corresponding time and temperature leading to Si–O bond formation in the Si-PETNC crystal during the heating process^a

Products	Reaction pathways	<i>t</i> (ps)	<i>T</i> (K)
Si–O bond	C ₁₃ H ₁₉ N ₉ O ₂₁ Si ₂ (49) → C ₁₃ H ₁₉ N ₉ O ₂₁ Si ₂ (51)	15.21	2353
	C ₄ H ₆ N ₂ O ₆ Si (70) + HO (66) → C ₄ H ₇ N ₂ O ₇ Si (71)	15.49	2391
	CH ₂ O (106) + CH ₄ O ₃ Si (134) → C ₂ H ₆ O ₄ Si (142)	16.33	2505
	C ₄ H ₇ N ₂ O ₆ Si (150) + CHN ₂ O ₄ (126) → C ₄ H ₇ N ₂ O ₇ Si (155) + CHN ₂ O ₃ (158)	16.48	2525
	C ₃ H ₄ NO ₄ (191) + C ₃ H ₄ N ₂ O ₃ Si (177) → C ₂ HNO ₂ (192) + C ₄ H ₇ N ₂ O ₅ Si (193)	16.80	2568
	C ₂ H ₄ OSi (222) + C ₅ H ₈ O ₄ Si (231) → C ₇ H ₁₂ O ₅ Si ₂ (249)	17.21	2623
	C ₅ H ₃ N ₃ O ₇ Si (289) + HONO (181) → C ₅ H ₄ N ₄ O ₉ Si (291)	17.54	2668
	C ₅ H ₁₀ O ₂ Si ₂ (281) + NO ₂ (182) → C ₅ H ₁₀ NO ₄ Si ₂ (306)	17.61	2677
	C ₂ H ₂ NO ₂ (299) + CHNO ₄ Si (307) → C ₃ H ₃ N ₂ O ₆ Si (317)	17.68	2687
	C ₆ H ₁₁ NO ₆ Si ₂ (308) + HO (309) → C ₆ H ₁₂ NO ₇ Si ₂ (323)	17.75	2696
	CH ₂ O (251) + C ₆ H ₁₂ NO ₇ Si ₂ (323) → C ₇ H ₁₄ NO ₈ Si ₂ (333)	17.87	2712
	C ₇ H ₁₄ N ₂ O ₉ Si ₂ (364) + CH ₂ O ₂ (268) + NO ₃ (353) → C ₈ H ₁₅ N ₂ O ₁₁ Si ₂ (366) + HNO ₃ (365)	18.19	2756
	C ₅ H ₈ O ₉ Si ₂ (399) + C ₂ H ₃ O (389) → C ₇ H ₁₁ O ₁₀ Si ₂ (411)	18.60	2811

^a The numbers in parentheses are the identifications (ID) of the fragments.

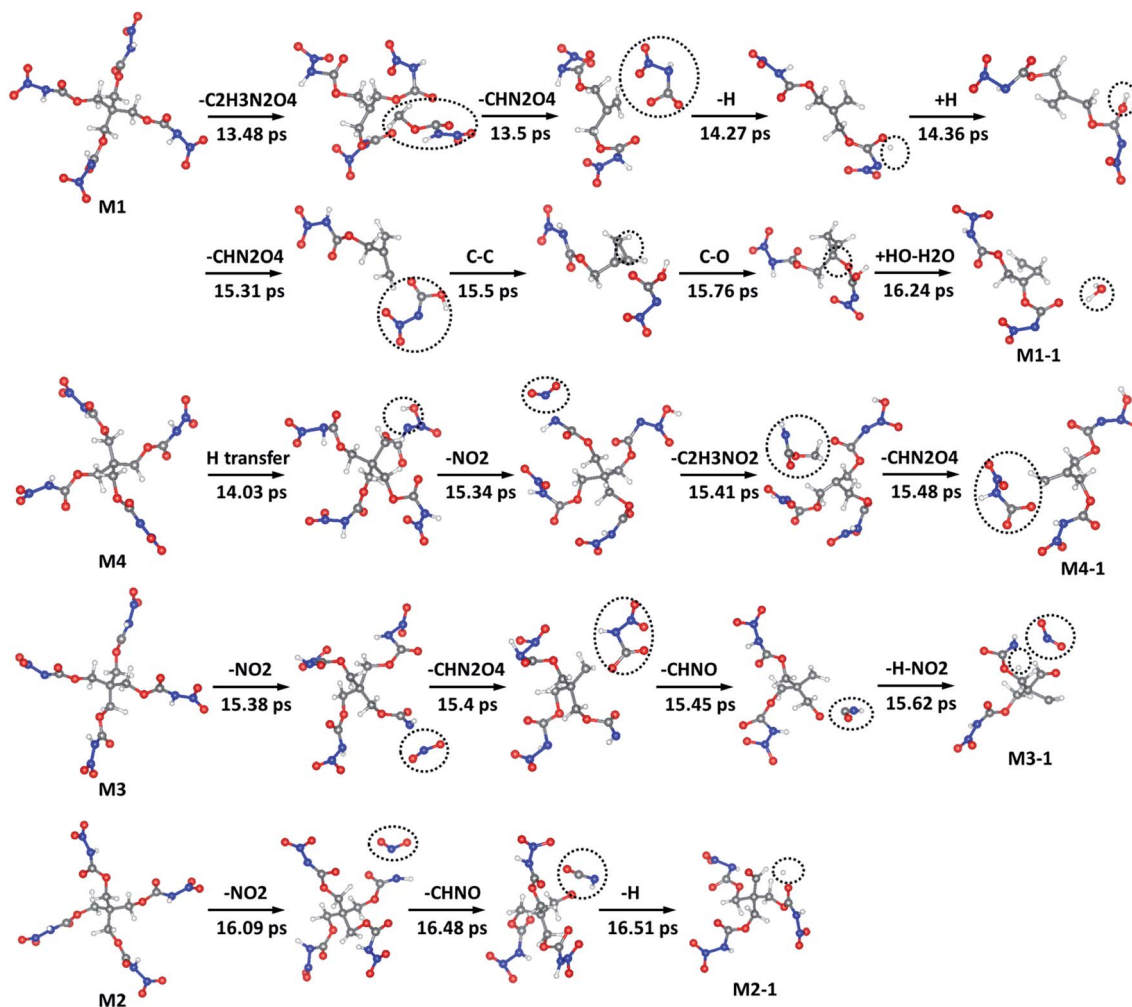


Fig. 6 Reaction process of initial reactions during the thermal decomposition of PETNC. The C, H, N, and O atoms are represented by gray, white, blue, and red balls, respectively.

the only $\text{C}_2\text{H}_3\text{N}_2\text{O}_4$ formed during the whole heating process for PETNC. We did not observe the dissociation of $\text{C}_2\text{H}_3\text{N}_2\text{O}_4$ in the decomposition of Si-PETNC. The $\text{CH}_2\text{-O}$ bond breaks just after $\text{C}_2\text{H}_3\text{N}_2\text{O}_4$ dissociation, leading to the formation of CHN_2O_4 at 2123 K ($t = 13.5$ ps). This CHN_2O_4 is also unstable, quickly decomposing to CO_2 and HN_2O_2 . In comparison with Si-PETNC, CHN_2O_4 forms ~ 2 ps earlier and at a temperature ~ 270 K lower for PETNC, making it more important in the initial decomposition of PETNC. The following reaction is the elimination of H from $-\text{NH}$ at 2226 K ($t = 14.27$ ps), which is rapidly consumed by the attraction of the O in $-\text{CO}$ within the same branch.

For M4, the first reaction step is H transfer between the H in $-\text{NH}$ and one O in $-\text{NO}_2$ when the temperature approaches 2194 K ($t = 14.03$ ps). However, this H transfer does not promote the dissociation of HONO or HO. Instead, the decomposition of this molecule occurs through NH-NO_2 bond cleavage in another branch at 2371 K ($t = 15.34$ ps). This is identical to the intramolecular H transfer in Si-PETNC. The following reactions of C-CH_2 and $\text{CH}_2\text{-O}$ bond breakage occur quickly after NO_2 dissociation, leading to the formation of $\text{C}_2\text{H}_3\text{NO}_2$ and CHN_2O_4 at 15.41 and 15.48 ps, respectively. $\text{C}_2\text{H}_3\text{NO}_2$ is unstable, and

immediately decomposes into CH_2O and CHNO . We did not observe $\text{C}_2\text{H}_3\text{NO}_2$ in the thermal decomposition of Si-PETNC. The initiation of M3 and M2 decomposition occurs *via* NH-NO_2 bond rupture that generates NO_2 when the temperature reaches 2376 K ($t = 15.38$ ps) and 2472 K ($t = 16.09$ ps), respectively. The subsequent reactions for M3 include the dissociation of CHN_2O_4 , CHNO , H, and the second NO_2 . For M2, CHNO and H elimination are the next reactions. The reaction details of these initial products and their evolution with temperature/time are described in Fig. S6 of the ESI.†

Unlike Si-PETNC, only one C-O bond is formed during the whole thermal decomposition process of PETNC. It is formed due to the attraction between the central C and one O in the dissociated CHN_2O_4 when the temperature reaches 2428 K ($t = 15.76$ ps) in one thoroughly decomposed PETNC molecule (M1 as shown in Fig. 6). No $\text{C-CH}_2\text{-O}$ rearrangement is detected for PETNC due to the large branch that is difficult to bend and the high barrier of this reaction. Therefore, C-O bond formation does not play an important role in the decomposition of PETNC, which is a significant difference between the initial reactions of Si-PETNC and PETNC.

When the temperature increases to ~ 2500 K, increments of various intermediate products, including HONO, $\text{H}_2\text{N}_2\text{O}_2$, $\text{CH}_2\text{N}_2\text{O}_4$, NO, HO, CNO, HNO, and N_2O_2 , are detected. The further decomposition of the initial products as well as PETNC moieties and the secondary reactions between products lead to the formation of these intermediates. The final products formed during the thermal decomposition of PETNC include CO_2 , CO, H_2O , N_2O , H_2 , and N_2 . The evolution of major reaction products with temperature/time is presented in Fig. S6 of the ESI.†

3.3 The origins for the higher sensitivity of silicon analogs and the lower sensitivity of nitrocarbamates

Energetic molecular solids can rapidly transition from slow thermal decomposition to rapid, self-sustained reactions that lead to thermal runaway and explosion.^{61,62} Because the initial decomposition is endothermic, the internal energy release and increased violence of reaction are delayed until the onset of exothermic reactions, which are thus of paramount importance to the safety of EMs.⁶³ We consider that the variation of energy under external stimuli is crucial to the understanding of the sensitivity of EMs since it correlates closely with the violence of initial endothermic reactions and secondary exothermic reactions. Thus we consider that the temperature programmed reaction dynamics provide a more reliable measurement of sensitivity than considering just one or two specific factors such as molecular electro-negativity and the weakest bond dissociation energy.

Fig. 7 shows the potential energy variations with temperature/time during the thermal decomposition process under heating for Si-PETN, PETN, Si-PETNC, and PETNC. For the nitro esters Si-PETN and PETN, the evolution of potential energy can be partitioned into two stages: energy accumulation and then energy release. For Si-PETN, the energy increases from the beginning to ~ 11.3 ps and the corresponding temperature is 1826 K. The starting point of energy release agrees well with the time at which the rapid formation of Si–O bonds begins. Considering that the other two reactions occurring before 11.3 ps (NO_2 and CH_2O dissociation) are endothermic, we conclude that the energy release is from Si–O bond formation. For PETN, the energy release starts from 13.9 ps and the corresponding temperature reaches 2177 K, which matches very well with the time after which many intermediate and final products are generated due to secondary exothermic reactions between products. Thus, the onset of energy release begins earlier and at a much lower temperature for Si-PETN, in comparison with PETN.

Unlike the nitro esters, the evolution of potential energy for the nitrocarbamates Si-PETNC and PETNC occurs in three stages: a large increase in stage one followed by a short dynamic equilibrium in stage two and a decrease in stage three. For Si-PETNC, the energy increases within the first 15.15 ps ($T = 2345$ K) due to various initial endothermic reactions, followed by a dynamic equilibrium over the next 1.85 ps since some exothermic reactions occur. The energy begins to decrease after 17.0 ps ($T = 2595$ K), in excellent agreement with the time after which the rapid formation of Si–O bonds starts, indicating that Si–O bond formation contributes significantly to the energy

release of Si-PETNC. For PETNC, the first stage lasts for 15.7 ps ($T = 2420$ K), followed by a dynamic equilibrium during the next 1.9 ps. The energy release begins after 17.6 ps ($T = 2676$ K) due to the onset of more exothermic reactions that generate more intermediate and final products. Therefore, the energy is released earlier and at a lower temperature for Si-PETNC than for PETNC, which is consistent with the comparison between Si-PETN and PETN.

The difference in behavior between the carbon and silicon analogs indicates that the replacement of the central C atom by a Si atom accelerates thermal decomposition and energy release, making the Si analogs more sensitive. The high exothermicity of Si–O bond formation as an essential initial reaction in the decomposition of the Si analogs promotes the onset of other reactions including the decomposition of other products and the secondary reactions between products, leading to the generation of various intermediate and final products that release energy. This significantly accelerates the decomposition process and thus enhances the sensitivity.

Comparing the energy behaviors of the nitro esters and the nitrocarbamates, we find that the energy release begins much later and at much higher temperatures for the nitrocarbamates. The starting time and temperature are 13.9 ps and 2177 K for PETN, while they are 17.6 ps and 2676 K for PETNC. The decomposition of Si-PETN begins to release energy after 11.3 ps and the temperature is 1826 K, whereas the onset of energy release for Si-PETNC starts after 17.0 ps and the temperature approaches 2595 K. This indicates that the decomposition proceeds much more slowly and the exothermic reactions occur much later for the nitrocarbamates, making them less sensitive.

Another significant distinction is that the energy accumulated in stage one of the nitrocarbamates is much higher than that for the nitro esters, suggesting that nitrocarbamates need more energy to break the bonds in initial reactions. This implies that the nitrocarbamates have more initial reaction pathways that absorb energy or that the reaction barriers for the initial reactions are higher. Indeed, more endothermic reaction routes are observed in the initial decomposition of PETNC and Si-PETNC, compared to PETN and Si-PETN as shown in Table 3. This arises from the large and complex branch of the nitrocarbamate compounds that triggers various reaction channels. The common reaction product, NO_2 , is observed in the initial decomposition for all four EMs, but the reaction barriers for the nitrocarbamates are much higher. The reaction enthalpy for O– NO_2 bond dissociation in PETN and Si-PETN is 39.0 and 35.6 kcal mol^{-1} ,²⁴ while the reaction enthalpy for NH– NO_2 bond dissociation in PETNC and Si-PETNC approaches 48.6 and 48.2 kcal mol^{-1} with zero point energy (ZPE) correction from QM calculations at the level of M06/6-311G**. Hence, NO_2 is formed at a much higher temperature and the population is smaller for the nitrocarbamates than for the nitro esters, as shown in Fig. 8(a). Furthermore, the intervals between two initial reactions for PETNC and Si-PETNC are longer than those for PETN and Si-PETN, indicating that early reactions for the nitrocarbamates may not catalyze the following reactions and thus decomposition progresses more slowly. Although Si–O bond formation is observed for both Si-PETN and Si-PETNC, it

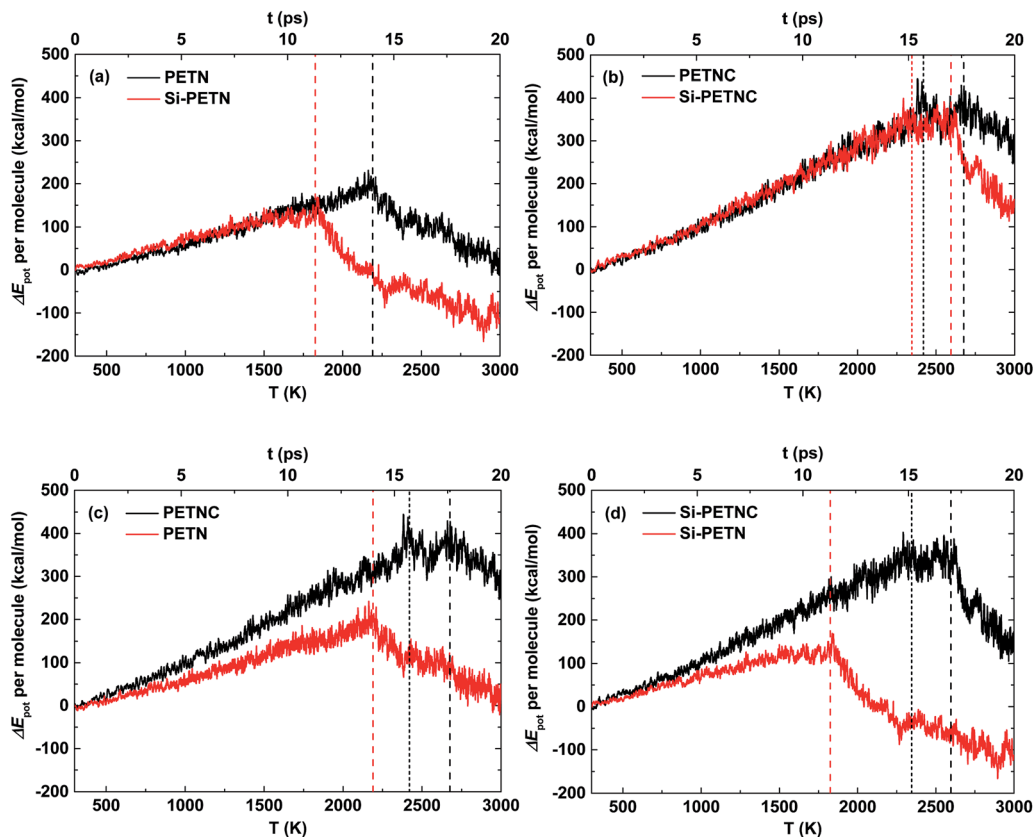


Fig. 7 Variation of potential energy with temperature/time during the thermal decomposition of Si-PETN, PETN, Si-PETNC, and PETNC. The data were normalized by the number of initial reactant molecules.

Table 3 The important initial reaction products formed during the thermal decomposition of Si-PETN, PETN, Si-PETNC, and PETNC. The corresponding formation time and temperature are included

Material	Product	<i>t</i> (ps)	<i>T</i> (K)
Si-PETN	NO ₂	9.21	1543
	CH ₂ O	9.25	1549
	Si–O bond	9.35	1562
PETN	NO ₂	13.17	2078
	HONO, H	13.24	2087
	CH ₂ O	13.31	2097
Si-PETNC	H transfer	10.19	1676
	NO ₂	12.72	2017
	H, HONO, CNO, CHNO	14.80	2298
	Si–O bond	15.21	2353
PETNC	C ₂ H ₃ N ₂ O ₄	13.48	2120
	CHN ₂ O ₄	13.50	2123
	H transfer	14.03	2194
	H	14.27	2226
	NO ₂ , CHNO, C ₂ H ₃ NO ₂	15.34	2371

occurs at a much higher temperature for Si-PETNC and the number is smaller as shown in Fig. 8(b). This is due to the large branch in the nitrocarbamates, which makes it more difficult to bend and rearrange the Si–CH₂–O and also impedes the attraction between the central Si and the O in dissociated products. Therefore, the role of Si–O bond formation in

enhancing the sensitivity of Si-PETNC is much less remarkable than for Si-PETN, making it much less sensitive. The subsequent equilibrium stage for the nitrocarbamates shows that the energy absorbed by endothermic reactions is still competitive with that released by exothermic reactions. This indicates that there are fewer secondary exothermic reactions or that the released energy is smaller for the nitrocarbamates, in comparison with the nitro esters.

3.4 Sensitivity evaluation

The experimental measurements^{23,27,28} presented in Table 4 for the four EMs suggest that

- thermal stability (T_{dec}) decreases in the order PETNC > Si-PETNC ≥ PETN > Si-PETN,
- impact sensitivity (IS) increases in the order PETNC < PETN ≤ Si-PETNC < Si-PETN, and
- friction sensitivity (FS) increases in the order PETNC < Si-PETNC < PETN < Si-PETN.

That is to say, when subjected to thermal, impact, or friction stimuli, Si-PETN is always the most sensitive one, and PETNC is always the most stable one. The thermal stability and impact sensitivity of Si-PETNC are similar to those of PETN, but the former exhibits lower sensitivity to friction. Overall, these experimental data indicate that

- the relative sensitivity of the four EMs increases in the order PETNC < Si-PETNC < PETN < Si-PETN.

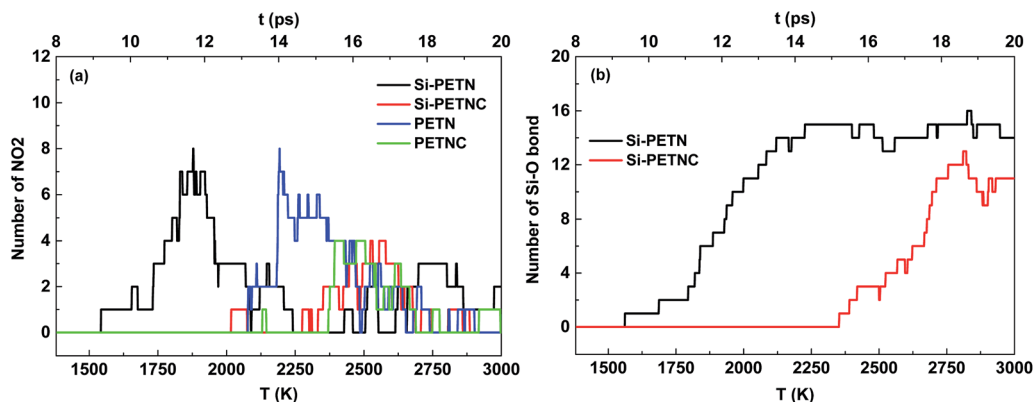


Fig. 8 Evolution with temperature/time of NO₂ and Si–O bonds formed during the thermal decomposition of Si-PETN, PETN, Si-PETNC, and PETNC.

Table 4 The relative sensitivity of PETN, PETNC, Si-PETN, and Si-PETNC^a

	Si-PETN	PETN	Si-PETNC	PETNC
t_{ini} (ps)	9.21	13.17	10.19	13.48
T_{ini} (K)	1543	2078	1676	2120
$t_{\text{endo-exo}}$ (ps)	11.30	13.90	17.0	17.60
$T_{\text{endo-exo}}$ (K)	1826	2177	2595	2676
ΔE_{endo} (kcal mol ⁻¹)	156	210	389	430
r_{exo} (ps ⁻¹)	0.31	0.09	1.01	0.19
T_{dec} (K)	298 ^b	438 ^c	443 ^d	469 ^c
IS (J)		3–4 ^c	3 ^d	8 ^c
FS (N)		60–80 ^c	240 ^d	360 ^c

^a t_{ini} , T_{ini} : the initiation time and the corresponding temperature of the first reaction step; $t_{\text{endo-exo}}$, $T_{\text{endo-exo}}$: the time/temperature at which the energy changes from endothermic to exothermic; ΔE_{endo} : the absorbed energy before energy release; r_{exo} : the rate of energy release. ^b From ref. 29, a significant degree of decomposition was observed after 12 hours in a solution of Si-PETN in 1,2-dichloroethane at 298 K. ^c From ref. 27. ^d From ref. 28; IS: impact sensitivity; FS: friction sensitivity; no experimental data about the IS and FS of Si-PETN are obtained due to its extraordinarily high sensitivity.

Together with the experimental data regarding sensitivity, we summarized some crucial parameters obtained from the thermal decomposition simulations of Si-PETN, PETN, Si-PETNC, and PETNC in Table 4, trying to find the correlation between the parameters and the relative sensitivity of EMs. These parameters include the initiation temperature/time of the first reaction step (T_{ini} or t_{ini}), the temperature/time at which the energy changes from endothermic to exothermic ($T_{\text{endo-exo}}$ or $t_{\text{endo-exo}}$), the absorbed energy before energy release (ΔE_{endo}), and the rate of energy release (r_{exo}). We find that $T_{\text{endo-exo}}$ (or $t_{\text{endo-exo}}$) and ΔE_{endo} correlate very well with the relative sensitivity of the four EMs, as shown in Fig. 9. The EM with lower $T_{\text{endo-exo}}$ (or earlier $t_{\text{endo-exo}}$) and smaller ΔE_{endo} exhibits higher sensitivity, while the one with higher $T_{\text{endo-exo}}$ (or later $t_{\text{endo-exo}}$) and larger ΔE_{endo} has lower sensitivity. Accordingly, our DFT-MD simulations suggest that

- the relative sensitivity of the four EMs increases in the order PETNC < Si-PETNC < PETN < Si-PETN,

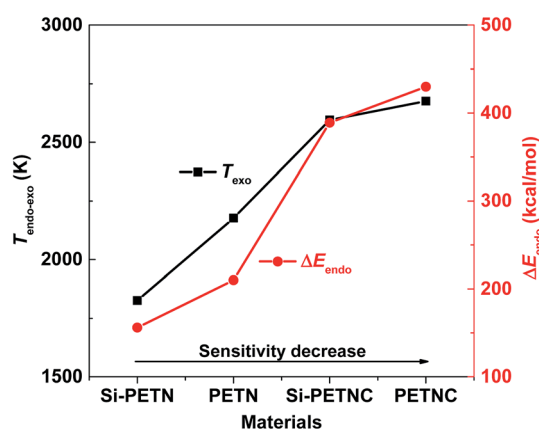


Fig. 9 Sensitivity correlation of the temperature at which the energy changes from endothermic to exothermic ($T_{\text{endo-exo}}$) and the absorbed energy before energy release (ΔE_{endo}) for Si-PETN, PETN, Si-PETNC, and PETNC. We find that $T_{\text{endo-exo}}$ and ΔE_{endo} both correlate very well with the relative sensitivity of the four EMs. The EM with lower $T_{\text{endo-exo}}$ and smaller ΔE_{endo} has higher sensitivity, while the one with higher $T_{\text{endo-exo}}$ and larger ΔE_{endo} exhibits lower sensitivity.

consistent with experimental result. Thus we propose that the temperature/time at which the energy changes from endothermic to exothermic and the absorbed energy before energy release correlate with the relative sensitivity of EMs, providing a simple tool for predicting the sensitivity of novel EMs prior to experimental synthesis and characterization. This criterion should provide guidance for developing new EMs with improved properties.

The initiation temperature/time of the first reaction step does not correlate with the relative sensitivity of the four EMs. For example, although the first reaction step occurs at a temperature 400 K lower (or ~ 3 ps earlier) for Si-PETNC than that for PETN, the former is less sensitive. The first reaction step (H transfer) occurring in Si-PETNC does not catalyze other reactions, showing little effect on enhancing the sensitivity. Therefore, we stress that it is necessary to find out whether the initial reaction promotes other reactions or not when using it to evaluate the sensitivity of EMs. Neither does the rate of energy

release r_{exo} correlate with the sensitivity of these EMs. r_{exo} is higher for the nitrocarbamates than for the nitro esters, which is the opposite of the relative sensitivity.

4. Conclusions

We used DFT-MD based temperature programmed reaction dynamics to determine the decomposition mechanisms of Si-PETN, PETN, Si-PETNC, and PETNC crystals to unravel the origins of the high sensitivity of the Si analogs (Si-PETN and Si-PETNC) and the low sensitivity of nitrocarbamates (Si-PETNC and PETNC). We also find a simple analysis that predicts the relative sensitivity of EMs.

The critical initial reaction products of Si-PETN include NO_2 , CH_2O , and the Si-O bond. The mechanisms leading to the formation of the Si-O bond involve the attraction between Si and the O from dissociated products, the rearrangement of Si- $\text{CH}_2\text{-O}$ in the partially decomposed Si-PETN molecule, and the intermolecular and intramolecular attractions between Si and one O in $-\text{NO}_2$. The attraction between Si and the O from dissociated products plays a predominant role in Si-O bond formation. The initial decomposition of PETN leads to the formation of NO_2 , HONO, H, and CH_2O .

For Si-PETNC, the crucial initial reactions include hydrogen transfer, dissociation of NO_2 , H, HONO, CNO, and CHNO , and Si-O bond formation. The intermolecular and intramolecular H transfers do not catalyze other reactions, and therefore do not accelerate the decomposition process. The mechanisms leading to the Si-O bond formation in Si-PETNC are similar to those in Si-PETN: the rearrangement of Si- $\text{CH}_2\text{-O}$ in the partially decomposed Si-PETNC molecule, the attraction between Si and the O from dissociated fragments, and Si attracting the O belonging to $-\text{CH}_2\text{O}$ in the adjacent Si-PETNC residue. The attraction between Si and the O from dissociated fragments plays a dominant role in the formation of the Si-O bond in Si-PETNC, identical to that for Si-PETN. The initial reactions for PETNC include the dissociation of $\text{C}_2\text{H}_3\text{N}_2\text{O}_4$ and CHN_2O_4 , intramolecular hydrogen transfer, and elimination of H, NO_2 , $\text{C}_2\text{H}_3\text{NO}_2$, and CHNO . The H transfer does not promote other reactions, the same as that for Si-PETNC.

In comparison with PETN and PETNC, the higher sensitivity of the Si analogs originates from the highly exothermic Si-O bond formation as a paramount initial reaction. It promotes other reactions including the decomposition of initial products and secondary exothermic reactions between products, leading to the generation of various intermediates and final products, thus accelerating the decomposition process and energy release and enhancing the sensitivity of Si-PETN and Si-PETNC.

The much lower sensitivity of nitrocarbamates compared to nitro esters is due to the large and complex branch of the reactant molecules. This large branch makes it more difficult to bend and rearrange the Si/C- $\text{CH}_2\text{-O}$ and also impedes the attraction between the central Si/C and the O in dissociated products. The Si-O bond forms at a higher temperature and the quantity is smaller for Si-PETNC compared to Si-PETN. The large complex branch also triggers more initial reaction channels that absorb energy and have higher reaction barriers. These

factors delay the onset of secondary reactions and energy release, thus lowering the sensitivity of Si-PETNC and PETNC.

The changes in potential energy under external stimuli provide an important measure for evaluating the sensitivity of EMs since it correlates closely with initial endothermic reactions and secondary exothermic reactions. We find that the temperature/time at which the energy changes from endothermic to exothermic ($T_{\text{endo-exo}}$ or $t_{\text{endo-exo}}$) and the accumulated energy before energy release (ΔE_{endo}) correlate very well with the relative sensitivity of the four EMs, making them useful criteria. The EM with lower $T_{\text{endo-exo}}$ (or earlier $t_{\text{endo-exo}}$) and smaller ΔE_{endo} has higher sensitivity, while the one with higher $T_{\text{endo-exo}}$ (or later $t_{\text{endo-exo}}$) and larger ΔE_{endo} exhibits lower sensitivity. Accordingly, the relative sensitivity of the four EMs predicted by our dynamical simulations increases in the order PETNC < Si-PETNC < PETN < Si-PETN, consistent with experimental results.

This study explains the increased sensitivity of Si analogs and the decreased sensitivity of nitrocarbamates of energetic molecules, providing mechanistic insight into the molecular and structural determinants that control the sensitivity of EMs. The proposed criteria related to energy variation under external stimuli provide a practical approach to predict the relative sensitivity of EMs prior to experimental synthesis and characterization. These findings should be useful in developing novel EMs with improved properties.

Conflicts of interest

The authors declare no conflicts of interest.

Acknowledgements

This work was supported by the National Natural Science Foundation of China (Grant No. 11402031 and 11521062) and ONR (N00014-16-1-2059 and N00014-12-1-0538, Cliff Bedford program manager).

References

- 1 T. M. Klapötke, *Chemistry of High-energy Materials*, De Gruyter, Berlin, 3rd edn, 2015.
- 2 T. Brinck, *Green Energetic Materials*, Wiley, New York, 2014.
- 3 J. P. Agrawal, *High Energy Materials: Propellants, Explosives and Pyrotechnics*, Wiley-VCH, Weinheim, 2010.
- 4 J. Giles, *Nature*, 2004, **427**, 580–581.
- 5 (a) A. A. Dippold and T. M. Klapötke, *J. Am. Chem. Soc.*, 2013, **135**, 9931–9938; (b) M. Göbel, B. H. Tchitchanov, J. S. Murray, P. Politzer and T. M. Klapötke, *Nat. Chem.*, 2009, **1**, 229–235; (c) T. M. Klapötke, C. Ptermayer, D. G. Piercy and J. Stierstorfer, *J. Am. Chem. Soc.*, 2012, **134**, 20827–20836; (d) D. Fischer, J. L. Gottfried, T. M. Klapötke, K. Karaghiosoff, J. Stierstorfer and T. G. Witkowski, *Angew. Chem., Int. Ed.*, 2016, **55**, 16132–16135; (e) T. S. Hermann, K. Karaghiosoff, T. M. Klapötke and J. Stierstorfer, *Chem.-Eur. J.*, 2017, **23**, 12087–12091.

- 6 (a) H. Gao and J. M. Shreeve, *Chem. Rev.*, 2011, **111**, 7377–7436; (b) J. Zhang, Q. Zhang, T. T. Vo, D. A. Parrish and J. M. Shreeve, *J. Am. Chem. Soc.*, 2015, **137**, 1697–1704; (c) Y. Liu, J. Zhang, K. Wang, J. Li, Q. Zhang and J. M. Shreeve, *Angew. Chem., Int. Ed.*, 2016, **55**, 11548–11551; (d) P. Yin, J. Zhang, L. A. Mitchell, D. A. Parrish and J. M. Shreeve, *Angew. Chem., Int. Ed.*, 2016, **55**, 12895–12897; (e) Y. Tang, J. Zhang, L. A. Mitchell, D. A. Parrish and J. M. Shreeve, *J. Am. Chem. Soc.*, 2015, **137**, 15984–15987; (f) V. Thottampudi, H. Gao and J. M. Shreeve, *J. Am. Chem. Soc.*, 2011, **133**, 6464–6470.
- 7 W. Zhang, J. Zhang, M. Deng, X. Qi, F. Nie and Q. Zhang, *Nat. Commun.*, 2017, **8**, 1–7.
- 8 D. G. Piercey, D. E. Chavez, B. L. Scott, G. H. Imler and D. A. Parrish, *Angew. Chem., Int. Ed.*, 2016, **55**, 15315–15318.
- 9 C. Zhang, C. Sun, B. Hu, C. Yu and M. Lu, *Science*, 2016, **355**, 374–376.
- 10 G. Bélanger-Chabot, M. Rahm, R. Haiges and K. O. Christe, *Angew. Chem., Int. Ed.*, 2015, **127**, 11896–11900.
- 11 Y. Tang, H. Yang, B. Wu, X. Ju, C. Lu and G. Cheng, *Angew. Chem., Int. Ed.*, 2013, **52**, 4875–4877.
- 12 U. Teipel, *Energetic Materials. Particle Processing and Characterization*, WILEY-VCH Verlag GmbH & Co. KGaA, 2005.
- 13 S. Iyer and N. Slagg, in *Structure and Reactivity*, ed. J. F. Liebman and A. Greenberg, VCH, New York, 1988, ch. 7.
- 14 C. B. Storm, J. R. Stine and J. F. Kramer, in *Chemistry and Physics of Energetic Materials*, ed. S. N. Bulusu, Kluwer, Dordrecht, The Netherlands, 1990, ch. 27.
- 15 R. Meyer, J. Köhler and A. Hornburg, *Explosives*, Wiley-VCH, Weinheim, 6th edn, 2007.
- 16 T. Zhou, J. Lou, Y. Zhang, H. Song and F. Huang, *Phys. Chem. Chem. Phys.*, 2016, **18**, 17627–17645.
- 17 C. Deng, X. Xue, Y. Chi, H. Li, X. Long and C. Zhang, *J. Phys. Chem. C*, 2017, **121**, 12101–12109.
- 18 Y. Ma, A. Zhang, X. Xue, D. Jiang, Y. Zhu and C. Zhang, *Cryst. Growth Des.*, 2014, **14**, 6101–6114.
- 19 J. Zhang, L. A. Mitchell, D. A. Parrish and J. M. Shreeve, *J. Am. Chem. Soc.*, 2015, **137**, 10532–10535.
- 20 V. J. Bellitto and M. I. Melnik, *Appl. Surf. Sci.*, 2010, **256**, 3478–3481.
- 21 H. Czerski and W. G. Proud, *J. Appl. Phys.*, 2007, **102**, 113515.
- 22 M. Huang, H. Z. Li, R. Xu, X. Q. Zhou, F. D. Nie and B. Chen, *Chin. J. Energ. Mater.*, 2011, **19**, 621–626.
- 23 T. M. Klapötke, B. Krumm, R. Ilg, D. Troegel and R. Tacke, *J. Am. Chem. Soc.*, 2007, **129**, 6908–6915.
- 24 W.-G. Liu, S. V. Zybin, S. Dasgupta, T. M. Klapötke and W. A. Goddard III, *J. Am. Chem. Soc.*, 2009, **131**, 7490–7491.
- 25 T. Zhou, L. Liu, W. A. Goddard III, S. V. Zybin and F. Huang, *Phys. Chem. Chem. Phys.*, 2014, **16**, 23779–23791.
- 26 B. W. Asay, B. F. Henson, L. B. Smilowitz and P. M. Dickson, *J. Energ. Mater.*, 2003, **21**, 223–235.
- 27 Q. J. Axthammer, B. Krumm and T. M. Klapötke, *Eur. J. Org. Chem.*, 2015, 723–729.
- 28 Q. J. Axthammer, T. M. Klapötke, B. Krumm and T. Reith, *Inorg. Chem.*, 2016, **55**, 4683–4692.
- 29 D. D. Dlott, *Mater. Sci. Technol.*, 2006, **22**, 463–473.
- 30 R. W. Armstrong, B. Baschung, D. W. Booth and M. Samirant, *Nano Lett.*, 2003, **3**, 253–255.
- 31 (a) J. T. Mang, R. P. Hjelm and E. G. Francois, *Propellants, Explos., Pyrotech.*, 2010, **35**, 7–14; (b) J. T. Mang and R. P. Hjelm, *Propellants, Explos., Pyrotech.*, 2011, **36**, 439–445.
- 32 Q. An, W. A. Goddard III, S. V. Zybin, A. J. Botero and T. T. Zhou, *J. Phys. Chem. C*, 2013, **117**, 26551–26561.
- 33 O. Sharia and M. Kuklja, *J. Am. Chem. Soc.*, 2012, **134**, 11815–18365.
- 34 M. J. Kamlet and H. G. Adolph, *Propellants, Explos., Pyrotech.*, 1979, **4**, 30–34.
- 35 (a) S. Zeman, in *Structure and Bonding*, ed. D. M. P. Mingos, Springer, Berlin, 2007; (b) S. Zeman, *J. Hazard. Mater.*, 2006, **132**, 155–164.
- 36 (a) P. Politzer and J. S. Murray, *Energetic Materials: Theoretical and Computational Chemistry Series*, Elsevier, New York, 2003, vol. 12; (b) P. Politzer and J. S. Murray, in *Energetic Materials, Part 2. Detonation, Combustion*, ed. P. Politzer and J. S. Murray, Elsevier, Amsterdam, 2003; (c) P. Politzer and J. S. Murray, *J. Mol. Struct.*, 1996, **376**, 419–424; (d) J. S. Murray, M. C. Concha and P. Politzer, *Mol. Phys.*, 2009, **107**, 89–97; (e) P. Politzer, J. S. Murray, J. M. Seminario, P. Lane, M. E. Grice and M. C. Concha, *J. Mol. Struct.: THEOCHEM*, 2001, **573**, 1–10; (f) J. O. Oxley, in *Energetic Materials, Part 1. Decomposition, Crystal and Molecular Properties*, ed. P. Politzer and J. S. Murray, Elsevier, Amsterdam, 2003, ch. 1.
- 37 (a) M. Pospíšil, P. Vávra, M. C. Concha, J. S. Murray and P. Politzer, *J. Mol. Model.*, 2010, **16**, 895–901; (b) M. Pospíšil, P. Vávra, M. C. Concha, J. S. Murray and P. Politzer, *J. Mol. Model.*, 2011, **17**, 2569–2574.
- 38 (a) L. E. Fried, M. R. Manaa, P. F. Pagoria and R. L. Simpson, *Annu. Rev. Mater. Res.*, 2001, **31**, 291–321; (b) S. M. Walley, J. E. Field and M. W. Greenaway, *Mater. Sci. Technol.*, 2006, **22**, 402–413; (c) C. J. Wu and L. E. Fried, *Proceed. 11th Int. Symp. Detonation*, Snowmass, CO, 1998.
- 39 (a) H. M. Xiao, W. H. Zhu, J. J. Xiao, G. X. Wang and X. Q. Pei, *Chin. J. Energ. Mater.*, 2012, **20**, 514; (b) W. Zhu and H. Xiao, *Struct. Chem.*, 2010, **21**, 657–665; (c) W. H. Zhu and H. M. Xiao, *J. Phys. Chem. B*, 2009, **113**, 10315–10321.
- 40 (a) E. A. Zhurova, A. Martin and A. A. Pinkerton, *J. Am. Chem. Soc.*, 2002, **124**, 8741–8750; (b) J. P. Ritchie, E. A. Zhurova, A. Martin and A. A. Pinkerton, *J. Phys. Chem.*, 2003, **B107**, 14576–14589.
- 41 B. M. Rice and J. J. Hare, *J. Phys. Chem. A*, 2002, **106**, 1770–1783.
- 42 D. Mathieu, *Ind. Eng. Chem. Res.*, 2017, **56**, 8191–8201.
- 43 S. A. Shackelford, *Cent. Eur. J. Energ. Mater.*, 2008, **5**, 75–101.
- 44 M. H. Keshavarz and M. Jaafari, *Propellants, Explos., Pyrotech.*, 2006, **31**, 216–225.
- 45 J. A. Morrill and E. F. C. Byrd, *J. Mol. Graphics Modell.*, 2008, **27**, 349–355.
- 46 M. M. Kuklja, Quantum-Chemical Modeling of Energetic Materials: Chemical Reactions Triggered by Defects, Deformations, and Electronic Excitations, *Adv. Quantum Chem.*, 2014, **68**, 71–146.

- 47 J. Trotter, Bond lengths and angles in pentaerythritol tetranitrate, *Acta Crystallogr.*, 1963, **16**, 698–699.
- 48 (a) W. Kohn and L. J. Sham, Self-Consistent Equations Including Exchange and Correlation Effects, *Phys. Rev.*, 1965, **140**, A1133; (b) P. Hohenberg and W. Kohn, Inhomogeneous Electron Gas, *Phys. Rev. B: Condens. Matter Mater. Phys.*, 1964, **136**, B864.
- 49 J. P. Perdew, K. Burke and M. Ernzerhof, *Phys. Rev. Lett.*, 1996, **77**, 3865–3868.
- 50 S. Grimme, S. Ehrlich and L. Goerigk, *J. Comput. Chem.*, 2011, **32**, 1456–1465.
- 51 (a) G. Kresse and J. Non-Cryst, *J. Non-Cryst. Solids*, 1995, **193**, 222–229; (b) G. Kresse and J. Furthmuller, *Comput. Mater. Sci.*, 1996, **6**, 15–50; (c) G. Kresse and J. Furthmuller, *Phys. Rev. B: Condens. Matter Mater. Phys.*, 1996, **54**, 11169–11186; (d) G. Kresse and D. Joubert, *Phys. Rev. B: Condens. Matter Mater. Phys.*, 1999, **59**, 1758–1775; (e) M. Hacene, A. Anciaux-Sedrakian, X. Rozanska, D. Klahr, T. Guignon and P. Fleurat-Lessard, *J. Comput. Chem.*, 2012, **33**, 2581–2589; (f) M. Hutchinson and M. Widom, *Comput. Phys. Commun.*, 2012, **183**, 1422–1426.
- 52 Q. An, Y. Liu, S. V. Zybin, H. Kim and W. A. Goddard III, *J. Phys. Chem. C*, 2012, **116**, 10198–10206.
- 53 Y. Lin, M. M. Budzevich, A. C. Landerville, I. I. Oleynik and C. T. White, *AIP Conf. Proc.*, 2009, **1195**, 474–477.
- 54 Y. A. Gruzdkov and Y. M. Gupta, *J. Phys. Chem. A*, 2000, **104**, 11169–11176.
- 55 W. L. Ng, J. E. Field and H. M. Hauser, *J. Appl. Phys.*, 1986, **59**, 3945–3952.
- 56 D. L. Naud and K. R. Brower, *J. Org. Chem.*, 1992, **57**, 3303–3308.
- 57 M. A. Hiskey, K. R. Brower and J. C. Oxley, *J. Phys. Chem.*, 1991, **95**, 3955–3960.
- 58 R. Behrens, *J. Phys. Chem.*, 1990, **94**, 6706–6718.
- 59 J. C. Oxley, M. Hiskey, D. Naud and R. Szekeres, *J. Phys. Chem.*, 1992, **96**, 2505–2509.
- 60 R. Behrens and S. Bulusu, *J. Phys. Chem.*, 1992, **96**, 8877–8891.
- 61 G. F. Adams and R. W. Shaw, *Annu. Rev. Phys. Chem.*, 1992, **43**, 311–340.
- 62 B. F. Henson and L. B. Smilowitz, in *Non-shock Initiation of Explosives*, ed. B. W. Asay, Springer-Verlag, Berlin, 2010, pp. 45–128.
- 63 V. I. Schweigert and S. E. Koh-Fallet, *J. Phys. Chem. A*, 2017, **121**, 1544–1552.